## Title

Investigating the Impacts of Roadway Activities on Fine Particle Concentrations Using Emerging Sensor Networks



## Author

Yoo, Kyongwon

## Publication Date

2023

Peer reviewed|Thesis/dissertation

UNIVERSITY OF CALIFORNIA

Los Angeles

# Investigating the Impacts of Roadway Activities on Fine Particle Concentrations Using Emerging Sensor Networks

A thesis submitted in partial satisfaction

of the requirements for the degree Master of Science

in Atmospheric and Oceanic Sciences

by

Kyongwon Yoo

2023

ABSTRACT OF THE THESIS

Investigating the Impacts of Roadway Activities

on Fine Particle Concentrations Using Emerging Sensor Networks

by

Kyongwon Yoo

Master of Science in Atmospheric and Oceanic Sciences

University of California, Los Angeles, 2023

Professor Suzanne E. Paulson, Chair

As car manufacturers have reduced vehicle tailpipe emissions, roadway sources of $PM_{2.5}$ (particulate matter with diameters $\leq 2.5$ μm) generated by brake wear, tire wear, and resuspended dust from the roadway have played an increasingly significant role in near-roadway exposure. In this study we used the spatially dense network of low-cost PurpleAir (PA) sensors. Approximately 400 sensors are deployed in Los Angeles County, with 22 located within 700 meters of a major roadway. Plotting the $PM_{2.5}$ concentrations for each PA sensor located within 700 meters of a roadway between January 2019 and December 2021 revealed no distance-decay trend. We then used the nearby personal weather stations to determine the hourly wind direction at each sensor and separated PM values according to whether they were downwind or upwind of their respective nearby roadways. The results showed that fine particles ($PM_{2.5}$) were elevated

within 240 meters of the roadway and decayed to the background concentration by 430 meters. The concentrations were 16 to 24% higher than the background concentration and were higher in periods of higher atmospheric stability and lower wind speeds.

The thesis of Kyongwon Yoo is approved.

Marcelo Chamecki

Jasper F. Kok

Suzanne E. Paulson, Committee Chair

University of California, Los Angeles

2023

*To my parents and friends…*

*who've been giving me much love*

*and support.*

TABLE OF CONTENTS

LIST OF FIGURES

LIST OF TABLES

# CHAPTER 1

## Introduction

Exposure to traffic-related air pollutants has been linked to an increased incidents of various adverse health outcomes such as cancer, adverse respiratory effects, asthma, general mortality, impaired immune function, type II diabetes, and heart attacks (Pearson et al., 2000; Van Der Vliet et al., 1997; Janssen et al., 2003; Hoek et al., 2002; Williams et al., 2009; Puett et al., 2011; Brugge et al., 2007). This has raised concerns about the health effects of air pollution. Of all the traffic-related air pollutants, particulate matter with aerodynamic diameter smaller than 2.5 μm ($PM_{2.5}$) is a significant contributor to the adverse health outcomes associated with exposure (Anderson et al., 2012; Pope & Dockery, 2006). In near-roadway environments, motor vehicle emissions from combustion, brake wear, tire wear, and resuspended dust by traffic movement have been observed to cause elevated concentrations of $PM_{2.5}$ (McCarthy et al., 2006; Jeong et al., 2019; Harrison et al., 2012; Oroumiyeh et al., 2022; Rutter et al., 2011). A significant proportion of the US population, (estimates range from 11% to 19%), lives close to major roadways (Brugge et al., 2007; Rowangould, 2013). Insufficient pollutant measurement monitors near roadways highlight the need for a higher spatiotemporal resolution to understand the impact of $PM_{2.5}$ exposure at the neighborhood scale.

To track compliance with the National Ambient Air Quality Standards (NAAQS) and safeguard public health, the United States federal and state environmental protection agencies utilize standard federal reference methods (FRM) or federal equivalent methods (FEM) to measure ambient $PM_{2.5}$ concentrations (Feenstra et al., 2019). However, the regulatory monitors'

ability to provide adequate spatial coverage for reflecting detailed $PM_{2.5}$ spatial and temporal variations near major roadways is limited by the high instrumentation and maintenance expense and strict siting criteria (Bi et al., 2020b, Rowangould, 2013). Recent advancements in low-cost sensor technology have opened new opportunities for measuring air quality beyond regulatory FRM/FEM monitors. Deploying these sensors in large numbers and their high frequency of measurement increases the spatiotemporal availability of measurements (Clements et al., 2017; Bulot et al., 2020). Although low-cost sensors allow for real-time air pollution monitoring at finer spatial and temporal scales, they are associated with significant limitations, primarily due to their lower accuracy than FRM/FEM monitors. One of the main challenges associated with low-cost sensors is their uncontrolled nature of sensor siting. This is because sensors are frequently owned and mounted by members of the general public and may not be placed or consistently maintained. This is a significant difference compared to the regulatory monitoring stations that are carefully sited and maintained. To address the limitations of low-cost sensors and ensure their accuracy and reliability in air pollution monitoring, quality control measures are required. AQ-SPEC, the South Coast Air Quality Management District Air Quality Sensor Performance Evaluation Center, has established standardized testing procedures for low-cost sensors in the field and laboratory settings. Through their comprehensive evaluation of multiple commercially available low-cost air quality sensors, they have determined that several sensors can perform effectively under ambient and controlled conditions (South Coast Air Quality Management District, 2022).

The PurpleAir-II (PA) sensor is a widely used low-cost sensor capable of providing real-time measurements for both outdoor and indoor levels of particulate matter (PM). The usage of PA has proliferated in the last few years; as of January 2022, more than 12,000 PA sensors are in

use worldwide (PurpleAir, 2022). AQ-SPEC conducted a field evaluation of the PA sensors and found that it correlates well (GRIMM: $R^2$ > 0.93; beta attenuation method (BAM): $R^2$ > 0.86; for 1-hr mean) with the FEM reference monitors for $PM_{2.5}$ measurements in Los Angeles (LA) area (AQ-SPEC, 2019). While the PA sensors demonstrate good performance in capturing daily and diurnal variations compared to FEM, they tend to overestimate $PM_{2.5}$ concentrations in a high-pollution environments (Gupta et al., 2018). Subsequently, the Environmental Protection Agency (EPA) compared PA sensor data and FEM and FRM measurements across 16 states. Their analysis revealed that PA sensors tend to overestimate concentrations of $PM_{2.5}$ by about 40%, but this discrepancy can be corrected by utilizing an optimized linear regression equation (Barkjohn et al., 2021).

The Health Effects Institute (HEI) conducted a systematic review to investigate the correlation between residential proximity to major roadways and the associated traffic-related air pollutants. The review identified a specific exposure zone within 300m to 500m from major roadways (HEI, 2010). Previous air pollution studies have often relied on roadway proximity as a proxy for elevated levels of transportation-related air pollutants. However, given the limited availability of regulatory monitors in certain areas of interest, this approach may not comprehensively assess air pollution levels.

The rate at which pollutants decay around roadways has been the subject of a number of studies (Karner et al., 2010; Choi et al., 2012; Hu et al., 2009).The appearance of decay curves downwind of roadways is a function of both the strength of the particle source, which controls the degree to which the pollutant concentration is elevated at the roadway edge, and the concentration of the pollutant in the background air (Choi et al., 2014). If there is a significant difference between the two, the pollutant will decay to background within a few hundred to a

few thousand meters, while if the two values are similar, the pollutant will decay to the background over a short distance (Hu et al., 2009; Choi et al., 2012; Choi et al., 2014). $PM_{2.5}$ is a relatively long-lived pollutant, as the material in the particles stays airborne for around a week. As a result, it has a higher background level relative to the traffic source, resulting in a shorter decay profile than observed for other traffic related pollutants such as ultrafine particle number or nitrogen oxides (Ranasinghe et al., 2019).

LA county, with a population of over 10 million residents and a population density of 2,467 people per square mile as of 2020, is the most populous county in the United States (US Census Bureau, 2020). The complex network of major roadways and freeways in LA, coupled with high traffic congestion results in increased exposure of nearby populations to elevated levels of traffic-related air pollution. However, current knowledge gaps and inaccuracies in air pollution assessments warrant further investigation. In this study, we employ PA sensors in Los Angeles and incorporate meteorological and traffic flow data to comprehensively investigate the extent to which $PM_{2.5}$ concentrations are elevated in the near-roadway environment. This research aims to provide a more thorough understanding of the air pollution exposure levels in areas proximate to major roadways and freeways, ultimately aiding in developing effective mitigation strategies.

# CHAPTER 2

# Methods

## 2.1 Study Region

We delimit our study region to LA county covering an area extending approximately from -118.607° to -117.682° in the West-East direction and from 33.688° to 34.323° in the South-North direction. From January 1, 2019, to Dec 31, 2021, there were 376 active outdoor PA sensors in our study region. However, it is essential to note that not all sensors consistently provided accurate measurements throughout the entire study period.

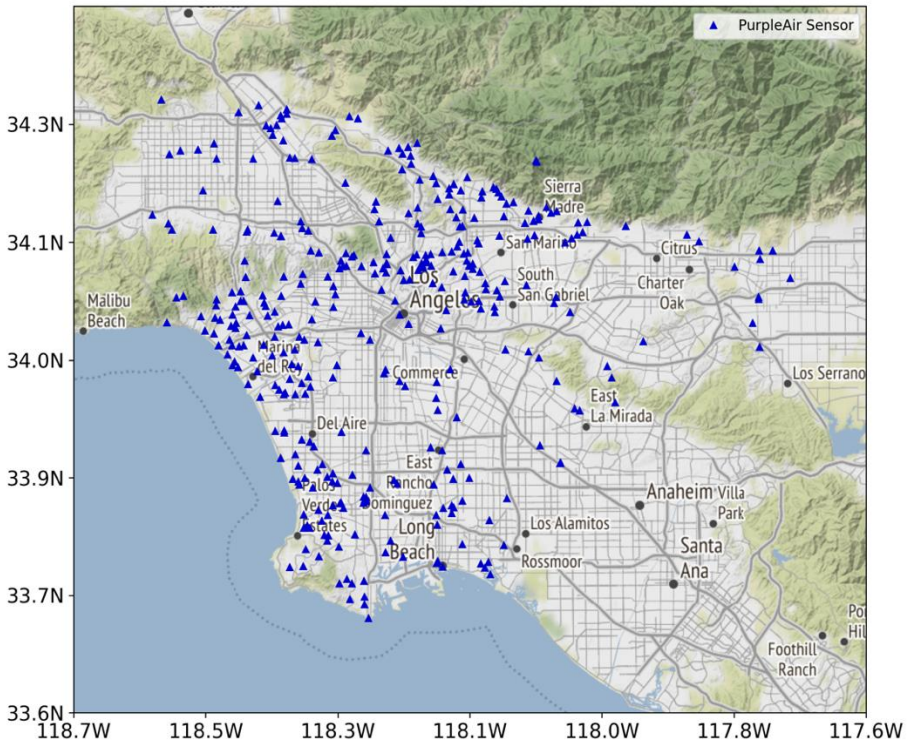


Figure 2.1: The study area of LA county, showing locations of PA sensors.

## 2.2 PurpleAir Sensor Data

### 2.2.1 PM2.5 Concentrations from the PurpleAir Sensor Network

Each PA sensor contains two Plantower PMS 5003 laser particle counters. PMS 5003 employs a fan to pull air past a laser beam, and the scattered light is detected at a 90-degree angle with a photo-diode detector. The detector converts the scattered light into a voltage pulse, and the number of particles in the air is determined by counting the number of pulses from the scattering signal (Sayahi et al., 2019). By identifying particles going past by their reflectivity, the PMS5003 sensors count suspended particles in sizes of 0.3, 0.5, 1.0, 2.5, 5.0, and 10 µm. The instrument has provided measurements of $PM_{1.0}$, $PM_{2.5}$, and $PM_{10}$ mass concentrations (µg $m^{-3}$), a proprietary algorithm that converts the counts to which it reports every 2-minutes. These values are reported in two ways, labeled CF=1 and CF=ATM. Additionally, the PA sensor contains BME280 environmental to monitor the chamber's inner relative humidity and temperature and an ESP8266 microcontroller to communicate with the PMS 5003 sensor and the PA server over Wi-Fi. PurpleAir presents the PM concentrations live on the PA map (PurpleAir, 2022). According to the manufacturer, each PMS5003 sensor has an effective measurement range of $PM_{2.5}$ concentrations between 0 and 500 µg $m^{-3}$, and working temperature and relative humidity ranges of -10 to 60 ℃ and 0 to 99 %, respectively (Yong & Haoxin, 2016).

### 2.2.2 Quality Assurance and Control for PurpleAir Data

There are several potential sources of error and issues with the quality of the data obtained from the PA network. To address this, we implemented quality assurance and quality control (QA/QC) per PurpleAir guidelines, as discussed in Connolly et al. (2022). The initial QA/QC steps included 1) removing observations for sensors with data from only one channel

and 2) removing data with temperature (T) and/or relative humidity (RH) that fall outside the PurpleAir acceptable range, 14 °F < T < 140 °F (-10 °C < T < 60 °C) and 0% < RH < 100%, respectively. Per the PurpleAir manufacturer's manual (Yong & Haoxin, 2016), we conducted further QA/QC on each PA sensor. Removing data with $PM_{2.5}$ mass concentrations exceeding 500 µg $m^{-3}$, and those for which the difference between the two channel readings exceeded ±10 µg $m^{-3}$ for averaged $PM_{2.5}$ readings below 100 µg $m^{-3}$, or greater than ±10% of the reading for averaged $PM_{2.5}$ readings above 100 µg $m^{-3}$. Additionally, we validated the outdoor designation of our sensors by creating time-series temperature plots. If the sensors showed a restricted temperature range, we inferred that they were actually indoor sensors mislabeled as outdoor and excluded them from further analysis.

To ensure the accuracy of the hourly averages, a 90% data completeness threshold was implemented for both channels A and B. Specifically, for measurements taken before May 30, 2019, which were based on 80-second intervals, an 80-second average was required to have at least 90% of the 45 data points available. For measurements taken after May 30, 2019, which were based on 120-second intervals, a 120-second average was required to have at least 90% of the 30 data points available. This approach aimed to establish reliable hourly averages and ensure consistency in data completeness thresholds across both sensor channels. Any data points that did not meet these requirements were not included in the calculation of the averages. Finally, sensors with more than 25% of total data failing QA/QC tests were removed from further analysis. Once cleaned, we obtained each sensor's final $PM_{2.5}$ mass concentrations by averaging measurements from channels A and B.

## 2.3 Meteorology Data

Using personal weather stations (PWS) for meteorological data acquisition has many advantages, including the ability to provide high spatial and temporal resolution data, and is often in closer proximity to the study area. Several websites, including Weathermap, WeatherLink, and Weather Underground, provide access to PWS data. As a result, these websites offer many locations for PWS data compared to traditional meteorological monitoring systems. In LA county alone, over 250 PWS were available during our study period. Although data obtained from PWS offer a high temporal and spatial resolution, it is important to address concerns about the quality and accuracy of such measurements. Therefore, we took several initial QC/QA measures to ensure that the PWS data used in this study were reliable. Additionally, we excluded data from PWS with a low data completeness from the analysis to maintain data quality. For our study area, we obtained meteorological data from two sources: the Weather Underground (IBM, 2019) and the EPA Air Quality System (AQS) database (https://www.epa.gov/air-data). We collected temperature (°F), relative humidity (%), wind speed (mph), and wind direction (°) parameters from the Weather Underground PWS at 5-minute intervals. In comparison, we found that the AQS database provided wind resultant data at an hourly average level consistent with PA $PM_{2.5}$ measurements. Since the Weather Underground data was recorded at a 5-minute resolution, we computed the hourly average of wind direction and wind speed using vector calculations.

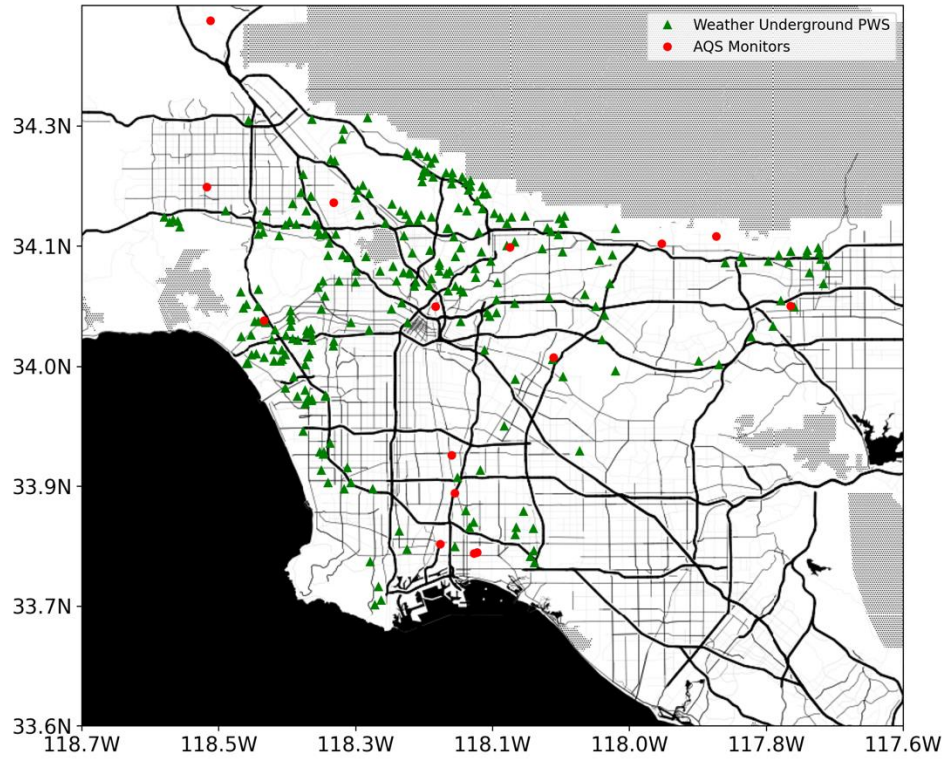


Figure 2.2: Weather Underground PWS and EPA AQS meteorological monitors in LA county.

### 2.3.1 Averaging Hourly Wind Speeds and Directions

To comprehensively represent the hourly wind conditions, we used the average vector method to determine the hourly average of wind speed and direction. This method involved computing resultant wind speed and direction by averaging each set of 5-minute Weather Underground wind speeds and direction measurements for the hour into a single hourly vector. As the wind is a vector quantity with both magnitude (wind speed) and direction (wind direction), this approach allowed us to capture both aspects of the hourly wind conditions. The wind speed vector components $u_i$ and $v_i$ for each 5-minute measurement, corresponding to east and north, are shown in Equations 2.1 and 2.2, respectively.

$$u_i = -s_i \times \sin\left[2\pi \times \frac{\theta_i}{360}\right] \quad (2.1)$$

$$v_i = -s_i \times \cos\left[2\pi \times \frac{\theta_i}{360}\right] \quad (2.2)$$

*where* $s_i$ and $\theta_i$ are the each 5-minute wind speed and direction measurements, respectively. Using Equations 2.1 and 2.2, we calculated the wind vector components by considering the magnitude of the wind speed ($s_i$). By meteorological convention, wind direction is defined as the direction from which the wind is blowing, whereas the vectors indicate the direction in which the wind is heading. Therefore, we added a negative sign to negate the direction and align with the convention. We averaged the wind speed vector components $u_i$ and $v_i$ over the one-hour averaging period to calculate the vector averages of wind speed.

$$\mathrm{V_E} = \frac{1}{\mathrm{N}} \sum_{\mathrm{i=1}}^{\mathrm{N}} u_i \quad (2.3)$$

$$\mathrm{V_N} = \frac{1}{\mathrm{N}} \sum_{\mathrm{i=1}}^{\mathrm{N}} v_i \quad (2.4)$$

From the sequence of N measurements of $u_i$, and $v_i$, we calculated the mean east-west component of wind, represented by $V_E$, and the mean north-south component, represented by $V_N$. To find the resultant vector average wind speed ($\bar{U}_{RV}$) and direction ($\bar{\theta}_{RV}$), we used Equation 2.5 and 2.6.

$$\bar{U}_{RV} = \sqrt{{V_E}^2 + {V_N}^2} \quad (2.5)$$

$$\bar{\theta}_{RV} = arctan2(V_E, V_N) + 180\,^{\circ} \tag{2.6}$$

Equation 2.6 assumes that the angle of the arctan2() function returns in degrees. To determine the direction of the wind, we used the arctan2() function. We added 180 degrees to convert the wind vector to the meteorological convention of the direction from which the wind is coming.

## 2.4 Traffic Data

Traffic emissions are an especially ubiquitous source of air pollution in the LA region, owing to a vast and complex network of freeways and highways. In this study, we utilized traffic flow data to better understand the spatial and temporal factors contributing to $PM_{2.5}$ sources associated with traffic. We acquired traffic flow data from the California Department of Transportation's (CalTrans) freeway performance measurement system (PeMS), which supplies historical and real-time information on traffic flow and speed through CalTrans vehicle detection stations (VDS). We identified the nearest VDS to the PA sensor location on each freeway (in one direction only) using OpenStreetMap (OSM). Subsequently, we aggregated the PeMS traffic data hourly to match the temporal resolution of PA $PM_{2.5}$ measurements.

# CHAPTER 3

# Data Analysis

## 3.1 Calibration of PurpleAir $PM_{2.5}$ Data

The South Coast AQMD conducted a field evaluation of the PA PM sensor (AQ-SPEC, 2019) and found that it demonstrates a good correlation with two regulatory monitors, the FEM BAM and GRIMM, for hourly $PM_{2.5}$ mass concentrations, as evidenced by $R^2$ values of 0.77 and 0.91, respectively. However, other studies have revealed a tendency for the PA sensors to overestimate $PM_{2.5}$ concentrations at higher relative humidity when compared to regulatory monitors (Tryner et al., 2020; Wallace et al., 2021; Magi et al., 2020). We identified PA sensors within 50m of active EPA AQS $PM_{2.5}$ monitoring sites to verify this potential overestimation further and refine the data. There were four PA sensors at four unique AQS monitoring sites near LA county.

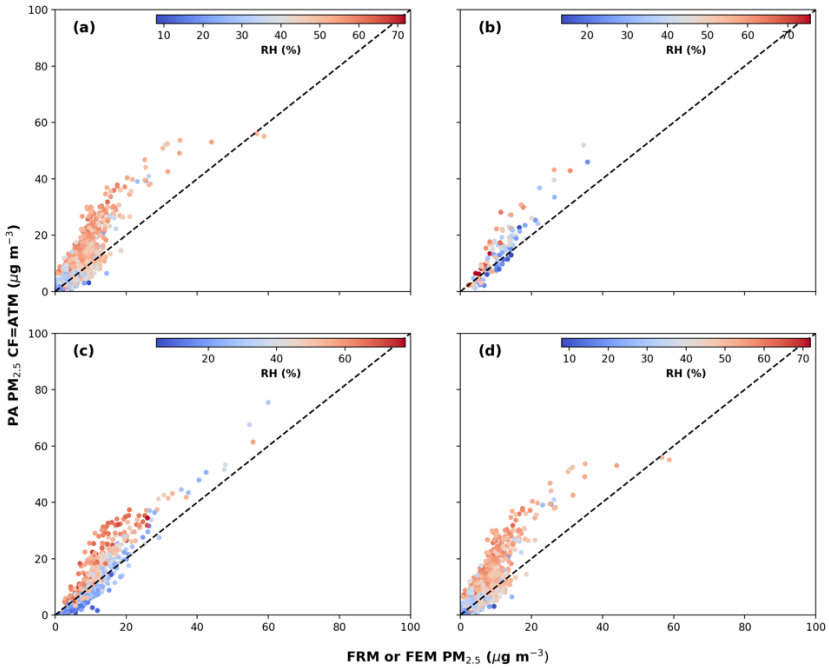


Figure 3.1: Comparison of 24h averaged raw PA $PM_{2.5}$ CF=ATM and FRM/FEM $PM_{2.5}$ measurements, with the 1:1 line in black dashed line. (a) - (b) are PA sensors located in Los Angeles, CA, (c) is in Riverside, CA, and (d) is Oxnard, CA.

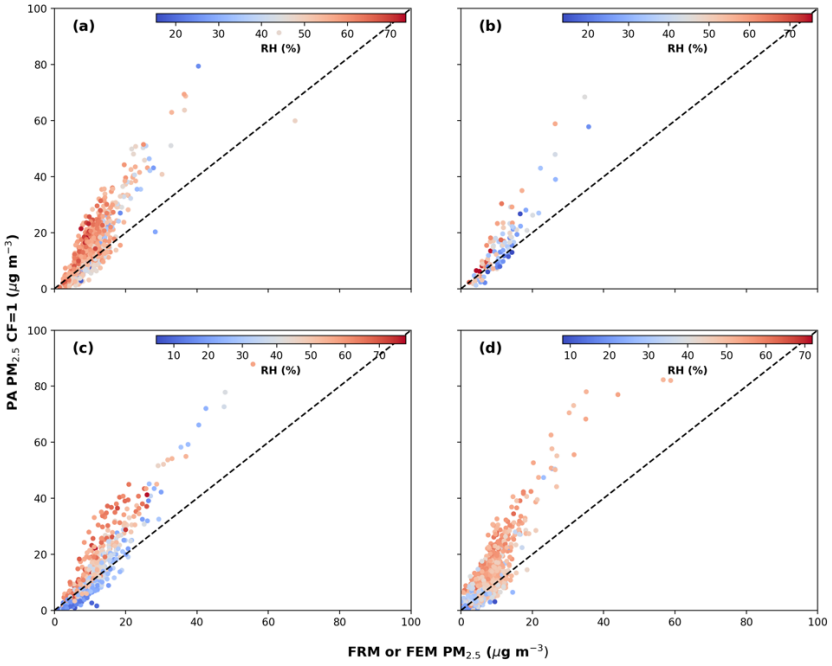


Figure 3.2: Comparison of 24h averaged raw PA $PM_{2.5}$ CF=1 and FRM/FEM $PM_{2.5}$ measurements, with the 1:1 line in black dashed line. (a) - (b) are PA sensors located in Los Angeles, CA, (c) is in Riverside, CA, and (d) is Oxnard, CA.

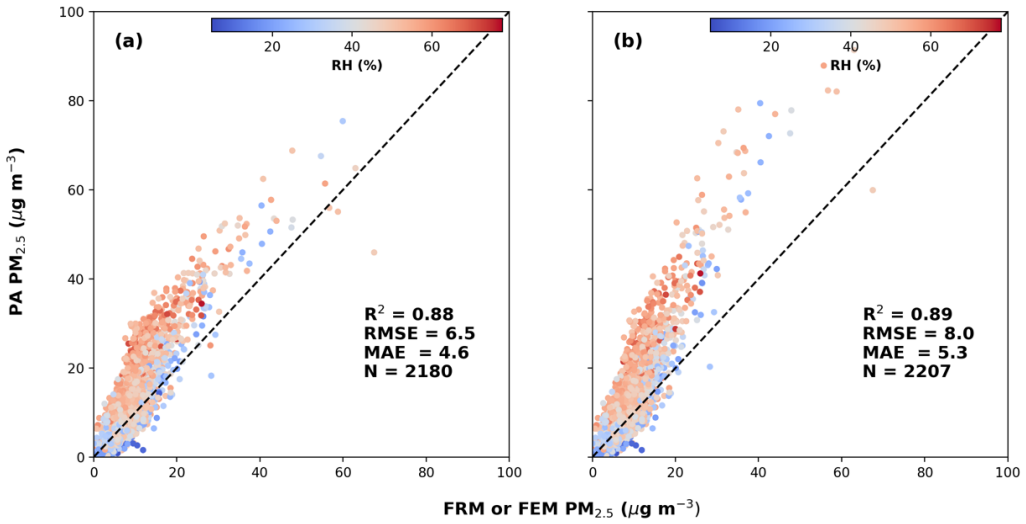


Figure 3.3: Comparison of 24-hour averaged (a) $PM_{2.5}$ CF=ATM and (b) $PM_{2.5}$ CF=1 measurements between four combined PA sensors and FRM/FEM measurements, with 1:1 line shown in black dashed line. Statistics included are the $R^2$, RMSE, MAE, and the number of 24-hour data points (N).

Figures 3.1 and 3.2 depict a comparison between 24-hour averaged PA $PM_{2.5}$ and FRM/FEM measurements, both at CF=1 and CF=ATM, for each location with respect to the corresponding regulatory monitor. We observed a lower root mean square error (RMSE) for the PA $PM_{2.5}$ with CF=ATM (RMSE = 6.50 µg $m^{-3}$) compared to $PM_{2.5}$ with CF=1 (RMSE = 8.0 µg $m^{-3}$). Figure 3.3 demonstrates that PA CF=ATM and CF=1 exhibits higher $PM_{2.5}$ concentrations than the values recorded by the regulatory monitor when the RH is high. Therefore, implementing corrections can further improve the accuracy of PA $PM_{2.5}$ measurements.

While prior research has developed a US-wide correction for $PM_{2.5}$ data (Barkjohn et al., 2021), our study focuses on the LA area in Southern California, and thus, we aim to utilize a collocated dataset in the same geographical region as our study area. We developed a data correction model for PA sensors by solely utilizing data reported by the PA sensors collocated with reference monitors, treating the 24-hour FRM/FEM $PM_{2.5}$ measurements as the independent

variable. Based on the analysis from Barkjohn et al. (2021), the three models with the lowest RMSE were considered. The equations displayed below are three selected models from Barkjohn et al. (2021). PA corresponds to the PurpleAir $PM_{2.5}$ data, while $PM_{2.5}$ represents to $PM_{2.5}$ measurements provided by the collocated FRM/FEM BAM monitors. The variables RH and T represent the relative humidity and temperature values measured by the PA sensors. In addition, the coefficient $m_1$ through $m_4$ are the fitted model coefficients, and b is the fitted model intercept.

1. Simple linear regression

$$PA = m_1 \times PM_{2.5} + b \quad (3.1)$$

2. Multilinear with an additive RH term

$$PA = m_1 \times PM_{2.5} + m_2 \times RH + b \quad (3.2)$$

3. Multilinear with additive and multiplicative terms using RH and T

$$PA = m_1 \times PM_{2.5} + m_2 \times RH + m_3 \times T + m_4 \times RH \times T + b \quad (3.3)$$

4. Multilinear with additive and multiplicative terms using RH and $PM_{2.5}$

$$PA = m_1 \times PM_{2.5} + m_2 \times RH + m_3 \times RH \times PM_{2.5} + b \quad (3.4)$$

### 3.1.1 Selecting Models

After applying the correction, we evaluated the effectiveness of the various correction models based on their ability to reduce both the RMSE and mean absolute error (MAE). Our analysis, as presented in Table 3.1, revealed that $PM_{2.5}$ CF=1 exhibited lower error than the CF=ATM data across all three models evaluated. Therefore, we opted to use the $PM_{2.5}$ CF=1

data to implement the correction to the $PM_{2.5}$ data, as it resulted in better model performance with a lower RMSE and MAE.

Table 3.1: Correction equation forms, RMSE, and MAE for PM2.5 24-hour average

| Name | Equation | CF=ATM ($\mu g$ m$^{-3}$) | | CF=1 ($\mu g$ m$^{-3}$) | |
|---|---|---|---|---|---|
| | | RMSE | MAE | RMSE | MAE |
| *Linear* | PA = m$_1$ × $PM_{2.5} + b$ | 3.73 | 2.85 | 3.29 | 2.47 |
| $+RH$ | PA = m$_1$ × $PM_{2.5} + m_2 \times RH + b$ | 3.41 | 2.60 | 3.06 | 2.29 |
| $+RH \times T$ | PA = m$_1$ × $PM_{2.5} + m_2 \times RH + m_3 \times T + m4 \times RH \times T + b$ | 3.32 | 2.48 | 2.93 | 2.16 |
| $PM \times RH$ | PA = m$_1$ × $PM_{2.5} + m_2 \times RH + m_3 \times RH \times PM_{2.5} + b$ | 3.29 | 2.47 | 2.99 | 2.22 |

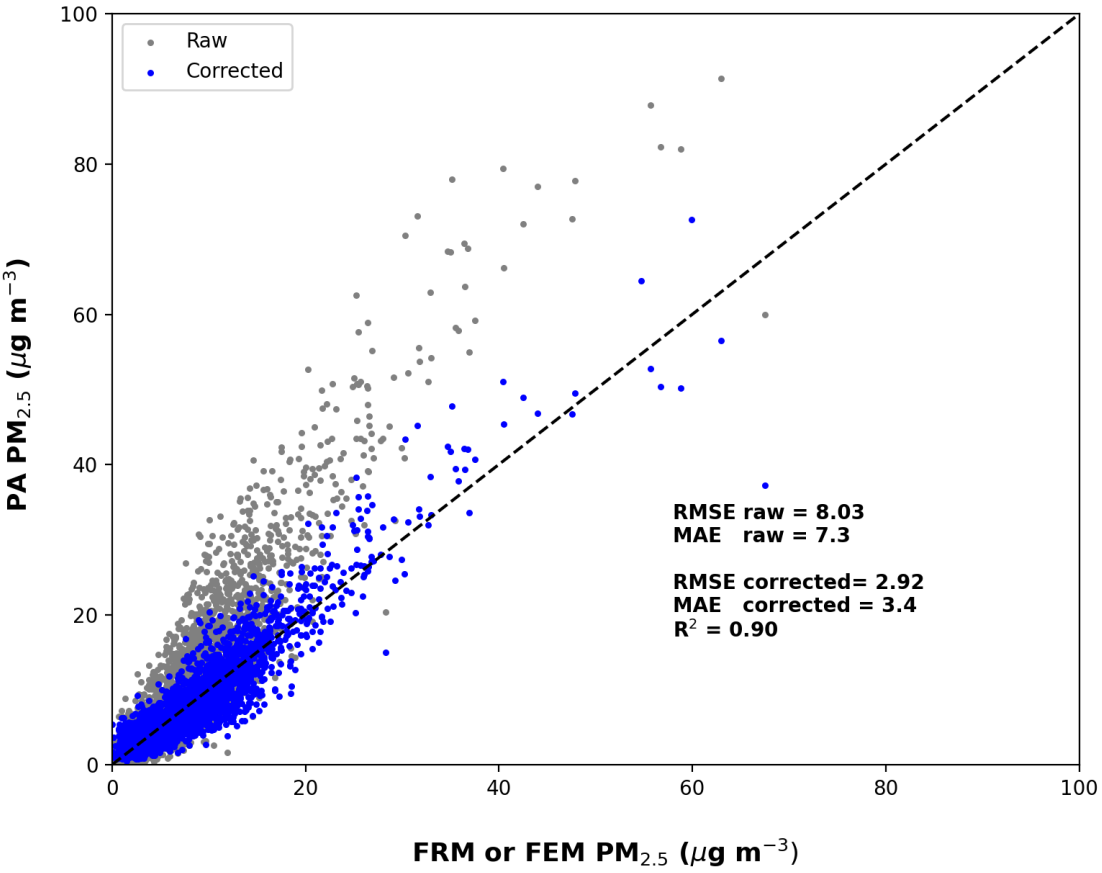


Figure 3.4: Comparison of 24-hour averaged raw PA $PM_{2.5}$ CF=1 versus FRM/FEM $PM_{2.5}$ measurements (gray) and corrected PA $PM_{2.5}$ CF=1 versus FRM/FEM $PM_{2.5}$ measurements (blue), with 1:1 line shown in black dashed line. Statistics included are the $R^2$, RMSE, and MAE.

Equation 3.3 yielded the lowest RMSE relative to the other correction models, with an RMSE of 2.93 µg $m^{-3}$. However, it is worth noting that Barkjohn et al. (2021) found the optimal option for reducing MAE on a wide range of data was the additive RH model (Equation 3.2). Nevertheless, because we are dealing with a specific area, we utilized a multilinear model with additive and multiplicative terms incorporating both RH and T factors (Equation 3.3). This approach may help account for the specific chemical and optical properties of aerosol in the LA area. We generated the following correction model (Equation 3.5) for the entire 1-hour averaged PA $PM_{2.5}$ data, where PA is the average of the A and B channels, T is in degrees Celsius, and RH is in percent.

$$PM_{2.5} = 0.602 \times PA_{cf=1} + 0.107 \times RH + 0.469 \times T - 0.00922 \times RH \times T - 4.64 \quad (3.5)$$

### 3.2 Data Screening

Accurately quantifying the contribution of traffic-related $PM_{2.5}$ to the near-road increment of $PM_{2.5}$ is crucial for our study. Nevertheless, a significant challenge in this assessment is the consideration of background concentration, which may confound the interpretation of near-roadway $PM_{2.5}$ concentrations. The positive correlation between background and near-roadway $PM_{2.5}$ concentration has been previously demonstrated in previous study (Askariyeh et al., 2020). Heightened background concentrations for a prolonged period can lead to the overestimation of the near-roadway $PM_{2.5}$ concentrations, irrespective of their proximity to the roadway.

During our study period, we observed elevated levels of $PM_{2.5}$ on July 4, 5, and New Year's Day, which were attributable to fireworks. Moreover, we utilized 9 FRM/FEM monitors

located in LA county to calculate a 5-day centered moving average (comprising the preceding two days and the following two days) of 24-hour $PM_{2.5}$ concentrations. We identified days when the 5-day moving average deviated significantly from the mean concentration, indicating anomalous pollution events. Consequently, these days were excluded from subsequent data analysis. The days excluded include the COVID-19 Shut down (03/07/2020 – 05/30/2020), Bobcat Fire (09/10/2020 - 09/19/2020) and (10/03/2020 - 10/07/2020), Los Angeles Port shut down (11/04/2021 - 11/07/2021), unknown event (12/01/2021 - 12/06/2021), Saddle Ridge Fire (10/10/2019 – 10/13/2019)

### 3.3 Data Visualization

This study investigates how changes in traffic and meteorological conditions, such as wind speed and direction, affect $PM_{2.5}$ concentrations as a function of distance from major roadways. We selected 44 of the 376 outdoor PA sensors within 700m of roadways for analysis, specifically those within 1000 meters of a PWS. The bearing angle of each PA sensor relative to the nearest roadways was calculated using OSM. The angle was perpendicular and at the minimum distance to the closest roadways. We categorized the hours as "downwind" when the 1-hour averaged wind direction was within a ± 45° arc (i.e., a 90° arc in total) perpendicular to the roadways and "upwind" when the wind direction was in the opposite direction of the roadways. To investigate whether wind direction significantly impacts the increment of near-road $PM_{2.5}$ compared to background concentrations, we classified all $PM_{2.5}$ concentrations and their associated wind directions into two classes: downwind and upwind. As depicted in Figure 3.5, the location of the PA sensor is displayed in proximity to the nearest roadways, along with the differentiated "downwind" and "upwind" wind direction categories.


Figure 3.5: Satellite view via Google Map of the near-roadway PA sensor site in Los Angeles, CA, with wind direction designation; red indicates angles included as upwind; blue indicates downwind.

Table 3.2 summarizes the PA sensors located within 700m of roadways, including the number of hours when the wind direction is in the downwind and upwind direction, $N_{Downwind}$ and $N_{Upwind}$. Specific rows in Table 3.2 were highlighted when the corresponding $N_{Downwind}$, or $N_{Upwind}$ was less than 10% of N total, the total observations. It is important to note that some of the sensor locations have a prevailing wind direction, which may result in a skewed distribution of $PM_{2.5}$ measurements in either the downwind or upwind direction. As a result, including these highlighted sensors when grouping them based on their proximity to each other and their distance from the roadways could potentially introduce bias when comparing the $PM_{2.5}$ concentrations in the downwind and upwind directions. Moreover, as these sensors are scattered throughout the general LA area, where pollution levels can vary widely, an uneven distribution of downwind or upwind data could introduce further bias into the dataset. Therefore, to ensure

the integrity of our analyses, we chose to exclude these 22 PA sensors from our subsequent analyses.

Table 3.2: Summary of the PA sensors dataset. N is total hours in downwind or upwind, and PA $PM_{2.5}$ concentration is summarized as mean(min, max). Highlighted rows are when downwind or upwind observations make up less than 10 percent of the total observations

| PA ID | Start date | End date | Distance to Roadway | $N_{Downwind}$ | $N_{Upwind}$ | PA $PM_{2.5}(\mu g/m^3)$ |
|---|---|---|---|---|---|---|
| 23089 | 02/05/21 | 12/31/21 | 50 m | 1,865 | 1,461 | 10.4 (0.0, 49.7) |
| 13967 | 06/01/20 | 12/31/21 | 80 m | 5,684 | 3,127 | 12.3 (0.3, 66.5) |
| 5844 | 01/02/20 | 12/30/21 | 90 m | 909 | 847 | 11.2 (0.1, 69.3) |
| 87129 | 12/06/20 | 12/30/21 | 130 m | 989 | 4,696 | 10.9 (0.3, 77.5) |
| 96273 | 12/23/20 | 12/31/21 | 150 m | 1,645 | 672 | 9.9 (0.0, 180.4) |
| 46941 | 01/27/20 | 12/31/21 | 160 m | 3,034 | 578 | 11.9 (0.2, 249.9) |
| 83465 | 12/31/20 | 12/30/21 | 170 m | 1,196 | 84 | 8.7 (0.0, 49.5) |
| 95367 | 12/31/20 | 12/31/21 | 190 m | 4,909 | 1,128 | 11.9 (0.4, 45.2) |
| 84107 | 10/21/20 | 12/31/21 | 200 m | 1,807 | 3,236 | 11.4 (0, 140.2) |
| 102032 | 03/23/21 | 12/30/21 | 210 m | 55 | 974 | 16.1 (0.0, 150.1) |
| 96423 | 12/28/20 | 12/30/21 | 220 m | 831 | 174 | 13.7 (0.4, 67.8) |
| 37551 | 11/30/21 | 12/31/21 | 220 m | 122 | 39 | 8.2 (0.1, 62.4) |
| 29215 | 03/27/19 | 12/31/21 | 270 m | 967 | 1,263 | 11.7 (0.3, 86.8) |
| 31541 | 09/25/20 | 12/31/21 | 270 m | 3,423 | 252 | 10.9 (0.1, 109.9) |
| 8994 | 04/03/19 | 12/30/21 | 280 m | 5,065 | 1,576 | 13.5 (0.1, 133.4) |
| 86193 | 11/08/21 | 12/30/21 | 290 m | 214 | 249 | 16.2 (0.4, 64.1) |
| 48397 | 02/19/20 | 12/31/21 | 290 m | 546 | 3,400 | 11.6 (0.2, 82.9) |
| 20700 | 01/03/19 | 12/31/21 | 300 m | 8,528 | 1,692 | 11.7 (0.0, 63.3) |
| 83647 | 10/27/20 | 12/31/21 | 330 m | 264 | 2,789 | 10.7 (0.3, 84.9) |
| 27109 | 08/24/19 | 12/31/21 | 400 m | 1,830 | 9,110 | 9.7 (0.1, 99.4) |
| 32339 | 05/23/19 | 12/30/22 | 410 m | 1,832 | 4,751 | 11.1 (0.0, 84.5) |
| 8922 | 06/01/20 | 08/02/21 | 410 m | 2,120 | 104 | 8.3 (0.9, 30.6) |
| 121123 | 08/17/21 | 12/30/21 | 420 m | 537 | 417 | 12.5 (0.0, 123.6) |
| 33855 | 11/14/21 | 12/31/21 | 420 m | 115 | 274 | 14.8 (0.2, 57.0) |
| 99139 | 09/25/21 | 12/30/21 | 420 m | 513 | 232 | 12.7 (0.1, 56.4) |
| 77543 | 10/11/20 | 12/31/21 | 420 m | 1,385 | 1,823 | 10.9 (0.1, 62.3) |
| 80455 | 10/16/20 | 12/31/21 | 450 m | 1,320 | 1,545 | 10.9 (0.1, 89.8) |
| 46937 | 01/27/20 | 12/31/21 | 460 m | 1,946 | 2,113 | 12.8 (0.1, 138.3) |
| 15901 | 01/02/19 | 12/31/21 | 510 m | 1,372 | 9,852 | 10.7 (0.0, 55.1) |
| 86071 | 11/06/20 | 12/30/21 | 530 m | 535 | 2,590 | 11.1 (0.0, 102.9) |
| 36143 | 10/20/20 | 12/30/21 | 530 m | 1,494 | 173 | 8.8 (0.1, 57.4) |
| 124961 | 12/25/21 | 12/30/21 | 540 m | 8 | 62 | 3.0 (0.1, 24.5) |
| 29229 | 08/14/19 | 12/31/21 | 560 m | 3,156 | 2,817 | 11.2 (0.1, 147.2) |
| 34495 | 09/20/21 | 12/31/21 | 560 m | 18 | 467 | 11.5 (0.0, 87.3) |
| 101081 | 03/10/21 | 12/31/21 | 560 m | 502 | 223 | 14.2 (0.0, 134.2) |
| 28515 | 03/12/19 | 12/31/21 | 580 m | 3,011 | 10,242 | 10.8 (0.1, 150.4) |
| 76759 | 10/08/20 | 12/30/21 | 590 m | 3,612 | 1 | 11.8 (0.1, 93.6) |
| 104908 | 05/19/21 | 10/29/21 | 590 m | 20 | 1,252 | 8.8 (0.1, 43.4) |
| 9156 | 08/10/20 | 12/31/21 | 590 m | 3,453 | 680 | 12.4 (0.1, 57.9) |
| 122949 | 12/11/21 | 12/31/21 | 630 m | 150 | 123 | 6.8 (0.0, 35.3) |
| 63387 | 08/28/20 | 12/31/21 | 680 m | 4,781 | 11 | 12.2 (0.4, 75.8) |
| 40721 | 07/24/20 | 12/31/21 | 690 m | 667 | 7,636 | 12.2 (0.1, 72.9) |
| 26505 | 10/01/20 | 12/31/21 | 700 m | 1,603 | 1,638 | 9.7 (0.1, 45.9) |
| 98179 | 05/19/21 | 12/31/21 | 700 m | 2,298 | 697 | 13.0 (0.2, 55.9) |

### 3.3.1 K-means Clustering

K-means clustering can effectively group sensors based on their proximity to the roadways. This approach is beneficial when dealing with large numbers of sensors scattered across a wide geographic area. This method can be used to investigate the spatial distribution of elevated $PM_{2.5}$ concentrations in each sensor cluster. Additionally, by averaging data from multiple sensors within each cluster, we can minimize the impact of any individual sensors that may be affected by local conditions or other factors. This study employed the K-means clustering method for 22 PA sensors. These sensors were grouped into four clusters based on their proximity to each other and their relative distance to the roadways (Figure 3.6, Table 3.3).


Figure 3.6: K-means clustering of PA sensors into four clusters. Centroids indicate the approximate center of each cluster in meters.

Table 3.3: Grouping the PA sensors dataset by using K-mean clustering

| Centroids | PA ID | Start date | End date | Distance to Roadway | $N_{Downwind}$ | $N_{Upwind}$ | PA $PM_{2.5}(\mu g/m^3)$ |
|---|---|---|---|---|---|---|---|
| 100 m | | | | | | | |
| | 23089 | 02/05/21 | 12/31/21 | 50 m | 1,865 | 1,461 | 10.4 (0.0, 49.7) |
| | 13967 | 06/01/20 | 12/31/21 | 80 m | 5,684 | 3,127 | 12.3 (0.3, 66.5) |
| | 5844 | 01/02/20 | 12/30/21 | 90 m | 909 | 847 | 11.2 (0.1, 69.3) |
| | 87129 | 12/06/20 | 12/30/21 | 130 m | 989 | 4,696 | 10.9 (0.3, 77.5) |
| | 46941 | 01/27/20 | 12/31/21 | 160 m | 3,034 | 578 | 11.9 (0.2, 249.9) |
| 240 m | | | | | | | |
| | 95367 | 12/31/20 | 12/31/21 | 190 m | 4,909 | 1,128 | 11.9 (0.4, 45.2) |
| | 84107 | 10/21/20 | 12/31/21 | 200 m | 1,807 | 3,236 | 11.4 (0, 140.2) |
| | 96423 | 12/28/20 | 12/30/21 | 220 m | 831 | 174 | 13.7 (0.4, 67.8) |
| | 8994 | 04/03/19 | 12/30/21 | 280 m | 5,065 | 1,576 | 13.5 (0.1, 133.4) |
| | 20700 | 01/03/19 | 12/31/21 | 300 m | 8,528 | 1,692 | 11.7 (0.0, 63.3) |
| 430 m | | | | | | | |
| | 27109 | 08/24/19 | 12/31/21 | 400 m | 1,830 | 9,110 | 9.7 (0.1, 99.4) |
| | 32339 | 05/23/19 | 12/30/22 | 410 m | 1,832 | 4,751 | 11.1 (0.0, 84.5) |
| | 121123 | 08/17/21 | 12/30/21 | 420 m | 537 | 417 | 12.5 (0.0, 123.6) |
| | 99139 | 09/25/21 | 12/30/21 | 420 m | 513 | 232 | 12.7 (0.1, 56.4) |
| | 77543 | 10/11/20 | 12/31/21 | 420 m | 1,385 | 1,823 | 10.9 (0.1, 62.3) |
| | 80455 | 10/16/20 | 12/31/21 | 450 m | 1,320 | 1,545 | 10.9 (0.1, 89.8) |
| | 46937 | 01/27/20 | 12/31/21 | 460 m | 1,946 | 2,113 | 12.8 (0.1, 138.3) |
| 610 m | | | | | | | |
| | 86071 | 11/06/20 | 12/30/21 | 530 m | 535 | 2,590 | 11.1 (0.0, 102.9) |
| | 29229 | 08/14/19 | 12/31/21 | 560 m | 3,156 | 2,817 | 11.2 (0.1, 147.2) |
| | 28515 | 03/12/19 | 12/31/21 | 580 m | 3,011 | 10,242 | 10.8 (0.1, 150.4) |
| | 26505 | 10/01/20 | 12/31/21 | 700 m | 1,603 | 1,638 | 9.7 (0.1, 45.9) |
| | 98179 | 05/19/21 | 12/31/21 | 700 m | 2,298 | 697 | 13.0 (0.2, 55.9) |

# CHAPTER 4

# Result and Discussion

## 4.1 Comparison of AQS monitors

### 4.1.1 Background Concentration

During our study period, nine AQS monitoring locations in LA county measured $PM_{2.5}$ concentrations using either FRM or FEM (Figure 4.1). Among the nine monitoring stations located in LA county, we identified three monitors (AQS 1602, 4002, and 4002) located within 600 meters of a roadway. Thus, they could not represent the background concentration as they were potentially affected by nearby emission sources. Two monitors (AQS 1302 and 4004) reported relatively elevated background $PM_{2.5}$ levels compared to the other areas, possibly due to local emission sources from oil refineries, railyards, and the Los Angeles Port, and these were also excluded. After excluding specific locations influenced by emissions sources, we identified four AQS monitoring locations (AQS 0002, 1103, 1201, and 2005) that were not impacted by local sources and were, therefore, suitable to represent background concentrations. Table 4.1 displays the mean 24-hour concentrations of $PM_{2.5}$ observed at each AQS monitor, along with the total number of days (N) used to calculate these means. The highlighted rows in the table correspond to four AQS monitoring locations identified as suitable background concentrations for subsequent analyses.

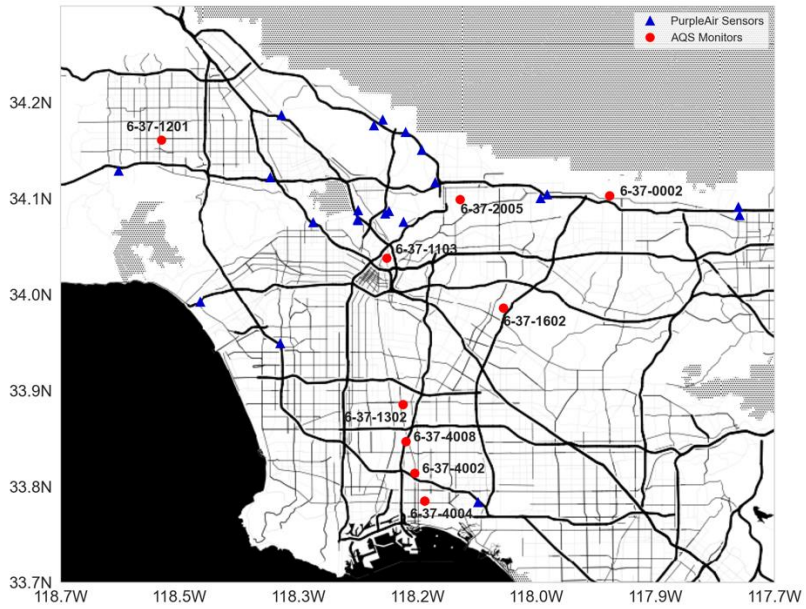


Figure 4.1: Locations of PA sensors and EPA AQS $PM_{2.5}$ monitors in LA county, CA.

Table 4.1: Statistic of 24-h $PM_{2.5}$ concentrations monitored at 9 stations in Los Angeles, CA

| | | | | | | Annual mean (µg/m$^3$) | | |
|---|---|---|---|---|---|---|---|---|
| AQS ID | FEM/FRM | Start date | End date | N | Mean (µg/m$^3$) | 2019 | 2020 | 2021 |
| 6-37-0002 | FRM | 01/03/19 | 12/27/21 | 320 | 10.5 | 9.2 | 12.4 | 10.5 |
| 6-37-1103 | FRM | 01/03/19 | 12/31/21 | 959 | 11.9 | 10.8 | 13.5 | 11.8 |
| 6-37-1201 | FRM | 01/03/19 | 12/30/21 | 317 | 9.5 | 8.9 | 10.8 | 9.1 |
| 6-37-1302 | FRM | 01/03/19 | 12/31/21 | 890 | 12.8 | 10.9 | 15.6 | 12.4 |
| 6-37-1602 | FRM | 01/03/19 | 12/30/21 | 322 | 12.0 | 10.3 | 14.7 | 11.8 |
| 6-37-2005 | FRM | 01/03/19 | 12/30/21 | 316 | 9.9 | 8.9 | 11.6 | 9.7 |
| 6-37-4002 | FRM | 01/02/19 | 12/30/21 | 356 | 10.3 | 9.0 | 12.7 | 10.3 |
| 6-37-4004 | Both | 01/02/19 | 12/31/21 | 962 | 11.8 | 9.9 | 14.2 | 11.9 |
| 6-37-4008 | FRM | 01/02/19 | 12/31/21 | 954 | 12.3 | 10.9 | 14.5 | 12.2 |

### 4.1.2 Near-Road PurpleAir Sensor Versus Background $PM_{2.5}$

Figure 4.2 presents box plots of $PM_{2.5}$ concentrations that contain data from 22 PA sensors for each group of five to seven PA sensors located in different bins of distance from the freeway. The data showed no clear trend with the distance to the nearest roadway. This indicates that on average the spatial distribution of $PM_{2.5}$ is predominantly influenced by factors other than proximity to vehicular traffic. Additionally, the mean background concentration of $PM_{2.5}$ measured by the AQS monitors ($\mu_{AQS}$) and the mean concentration measured by PA sensors ($\mu_{PurpleAir}$) is nearly identical; $\mu_{AQS}$ of 10.9 µg $m^{-3}$ and $\mu_{PurpleAir}$ of 11.4 µg $m^{-3}$.

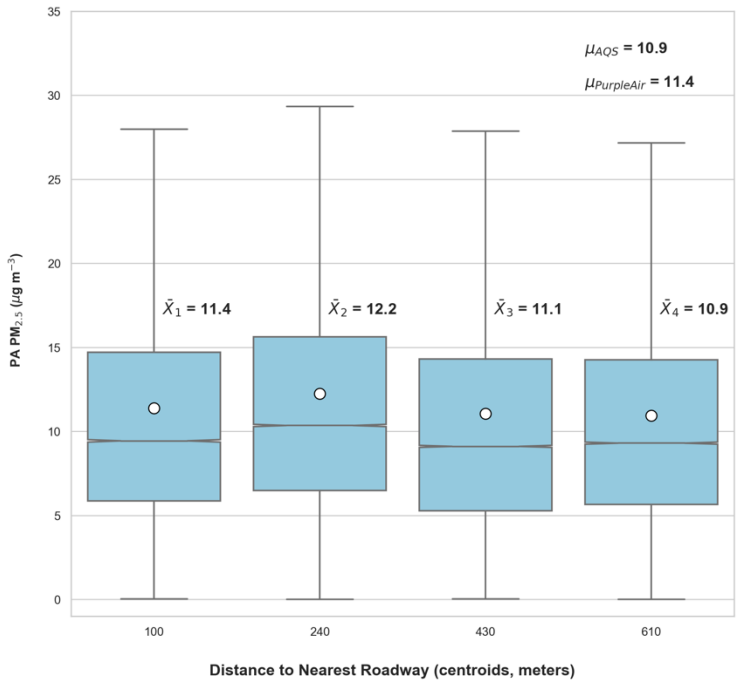


Figure 4.2: Boxplot of $PM_{2.5}$ concentrations (µg $m^{-3}$) with the distance to nearest roadway. The median is the horizontal line, the box contains the interquartile range, and the whiskers extend to the 10th and 90th percentiles. The mean of each boxplot is a white dot, the corresponding value is $\overline{X}_1$- $\overline{X}_4$, and the mean of PA and AQS background is $\mu_{PurpleAir}$ and $\mu_{AQS}$, respectively.

## 4.2 $PM_{2.5}$ Concentration, Wind Speeds, and Traffic Flow

### 4.2.1 $PM_{2.5}$ Concentrations: Downwind and Upwind

To analyze the extent to which downwind $PM_{2.5}$ concentrations are elevated compared to the background concentration, we will refer to upwind $PM_{2.5}$ concentration as the background concentration. The mean background concentration of the PA sensors was 10.6 µg $m^{-3}$, with the 100m centroid group exhibiting a slightly lower upwind concentration of 9.7 µg $m^{-3}$ (Figure 4.3). This difference can be attributed to several of the PA sensors in the group being located in a somewhat less polluted region, therefore the upwind $PM_{2.5}$ concentration was lower compared to other groups. The results in Figure 4.3 demonstrate that the mean concentration of $PM_{2.5}$ downwind of the 100m centroid group is higher than the background concentration, with a difference of 2.5 µg $m^{-3}$ (13.1 µg $m^{-3}$ and 10.6 µg $m^{-3}$ for downwind and background, respectively).

Furthermore, the downwind areas of the 240m centroid group also exhibited higher concentrations of $PM_{2.5}$ when compared to the background concentration, a difference of 1.7 µg $m^{-3}$. Our findings indicate that the level of downwind $PM_{2.5}$ concentration for both the 430m and 610m centroid groups were comparable to the background concentration, with a difference of less than 1.0 µg $m^{-3}$. This suggests that the increased distance from the roadways may have reduced the effects of $PM_{2.5}$ from traffic-related emissions. Nevertheless, wind speed and traffic flow can also influence $PM_{2.5}$ concentrations, leading to complex concentration patterns that do not rely solely on distance from the roadway.

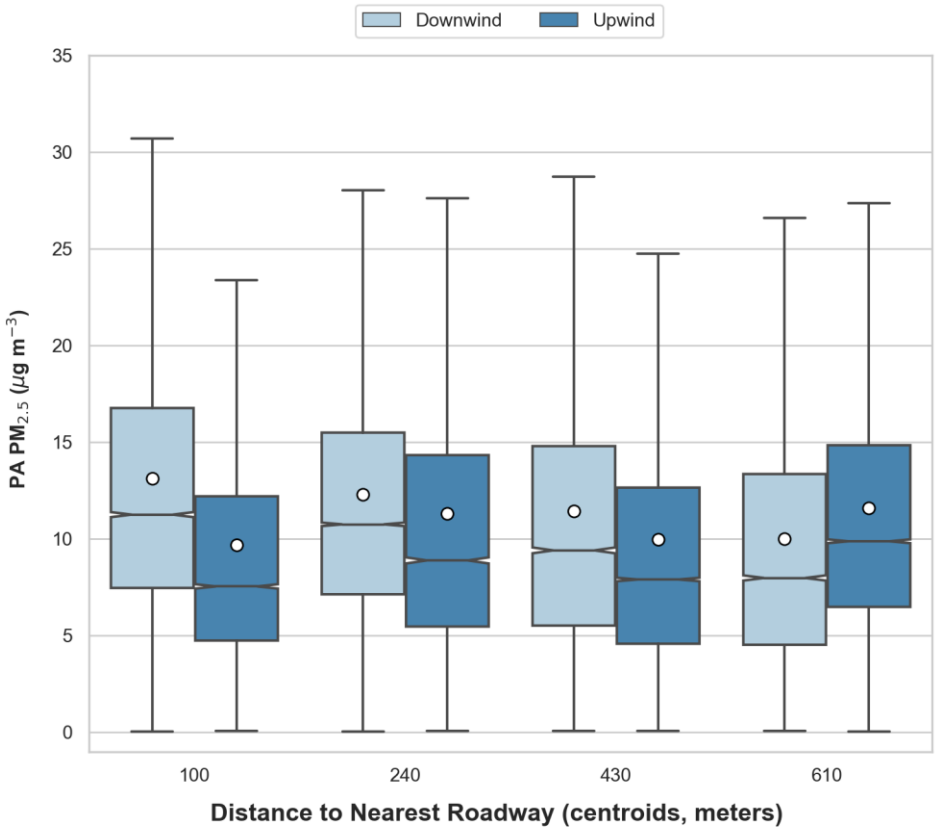


Figure 4.3: Boxplot of $PM_{2.5}$ concentrations (µg $m^{-3}$) with the distance to the nearest roadway for downwind and upwind cases. Whiskers indicate the range, circles the mean, indents the medians, and boxes the interquartile ranges.

### 4.2.2 Wind Speeds and Traffic Flow

Figure 4.4 presents the diurnal trend of downwind $PM_{2.5}$ concentrations with wind speed and traffic flow. Relatively lower wind speed and higher traffic flow are responsible for the observed surge in $PM_{2.5}$ concentrations during morning rush hours. Low wind speed during this period hinders the effective dispersion of $PM_{2.5}$ emissions, leading to its accumulation in the surrounding air. Concurrently, increased traffic flow results in the higher exhaust of $PM_{2.5}$ being released into the atmosphere. However, with increased wind speed, turbulent mixing in the mixed layer (ML) increases, causing the ML to thicken as air from high altitudes mixes with the

low levels. The ML height is a crucial determinant of pollutant dispersion, including $PM_{2.5}$. The increase in wind speed throughout the day causes the ML to grow and dilutes the concentration of $PM_{2.5}$. This phenomenon is responsible for the observed decrease in $PM_{2.5}$ concentration during the midafternoon, despite high traffic flow. After sunset, the Earth's surface cools, creating a surface temperature lower than the air above it, forming a stable boundary layer (SBL) with reduced vertical mixing. Low wind speeds and elevated traffic flow during the evening commute result in an observed increase in $PM_{2.5}$ concentration.

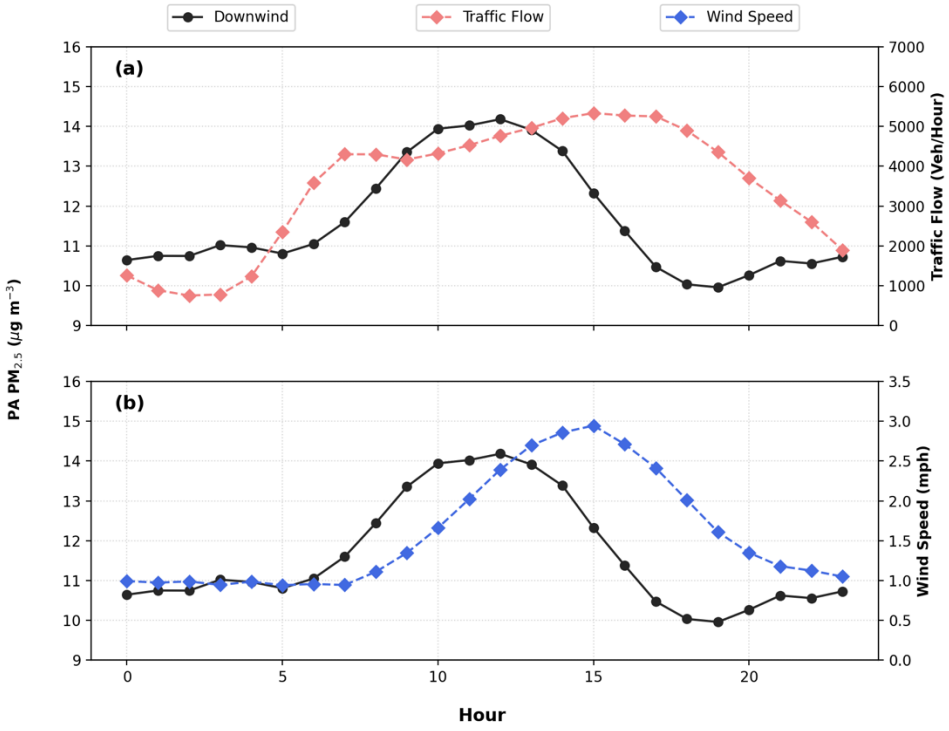


Figure 4.4: Diurnal variations (means) in the downwind $PM_{2.5}$ mass concentrations with a) traffic flow (vehicle/hour) and b) wind speed (mph).

## 4.3 Temporal and Spatial Variation of $PM_{2.5}$ Concentrations

Figure 4.5 illustrates the diurnal variation of $PM_{2.5}$ concentration for different centroid groups under downwind and upwind conditions. To highlight the impact of traffic flow on $PM_{2.5}$ concentration, we incorporated hourly traffic flow data for each centroid group (Figure 4.5 a–d). The findings suggest that the centroid group located 100 meters away consistently recorded higher $PM_{2.5}$ concentration levels than their upwind counterparts for all hours, with an average concentration difference of 3.2 µg $m^{-3}$. During afternoon peak traffic hours (13:00–15:00), the difference in concentration levels peaked at an average of 5.6 µg $m^{-3}$. The centroid group located 240 meters away also exhibited higher downwind concentrations from midnight to early morning (00:00–07:00). However, despite the higher traffic flow during afternoon hours, the difference in concentration levels between downwind and upwind was less extent that the 100m group.

The centroid group located 430 meters away generally exhibited comparable concentration levels between downwind and upwind. The most significant difference in concentration levels between downwind and upwind occurred during the early morning and early afternoon (03:00–07:00 and 09:00–15:00) when there was an increase in traffic flow from previous hours. The centroid group located 610 meters away showed lower downwind $PM_{2.5}$ concentrations for most hours compared to the upwind direction, except during morning and evening hours (10:00–12:00 and 20:00–22:00).

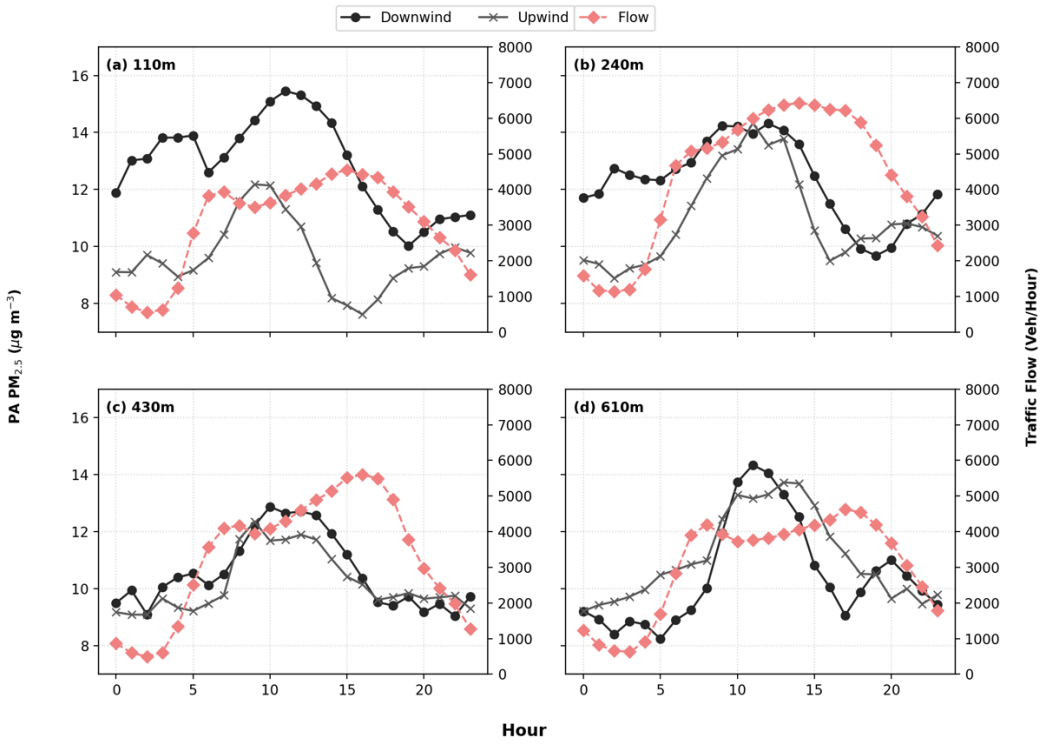


Figure 4.5: Temporal and spatial variations in the mean $PM_{2.5}$ mass concentrations of downwind and upwind centroid groups with traffic flow (vehicle/hour).

We investigated the difference in $PM_{2.5}$ concentrations between downwind and background under SBL and ML conditions. SBL conditions refer to the period between sunset and sunrise (19:00–06:00), whereas ML conditions refer to the period between sunrise and sunset (07:00–18:00). The focus of our investigation was to examine the mean differences in $PM_{2.5}$ concentrations between the downwind and background and assess the impact of SBL and ML conditions on the dispersion of $PM_{2.5}$ emissions from roadways. In the SBL and ML conditions, the PA sensors' mean upwind background concentrations were 9.6 µg $m^{-3}$ and 11.6 µg $m^{-3}$, respectively. We used Figures 4.6 (a) and 4.6 (b) to illustrate these differences.

Under the SBL conditions, the 100m and 240m centroid groups had elevated concentrations downwind compared to the background concentration. Specifically, the

downwind concentrations were 11.6 µg $m^{-3}$ and 11.5 µg $m^{-3}$ for 100m and 240m centroid groups, resulting in mean differences between downwind and background concentrations of 2.0 µg $m^{-3}$ and 1.9 µg $m^{-3}$, respectively. The observed differences in $PM_{2.5}$ concentrations between downwind and background can be attributed to the lower wind speeds, reduced turbulence, and decreased vertical mixing during SBL conditions. These conditions result in $PM_{2.5}$ accumulation near the roadway, leading to higher concentrations in the downwind region. Furthermore, the elevated traffic flow in the 240m centroid group may have contributed to the similar level of $PM_{2.5}$ concentration observed between the 100m and 240m centroid groups, even when located further away from the roadway. For the 430m and 610m centroid groups, the downwind and background concentrations were comparable, with a difference of less than 0.3 µg $m^{-3}$, suggesting that the traffic-related $PM_{2.5}$ did not disperse further downwind from the roadway under SBL conditions.

Under ML conditions, the 100m centroid group had the most significant difference in downwind and background concentrations, with a difference of 2.1 µg $m^{-3}$. This might be attributed to the shortest distance from the roadway, which was the most affected by traffic flow. The 240m centroid also had elevated $PM_{2.5}$ concentration relative to the background, with a difference of 1.2 µg $m^{-3}$. However, despite experiencing high traffic flow relative to the 100m centroid group, the impact of traffic flow on $PM_{2.5}$ levels in the 240m group was not significantly greater. For the 430m and 610m centroid groups, the downwind and background concentrations were also comparable, with a difference of less than 0.3 µg $m^{-3}$, suggesting that the traffic-related $PM_{2.5}$ did not disperse further downwind from the roadway under ML conditions.

We observed a consistent and linear decrease in downwind $PM_{2.5}$ concentrations from 13.7 µg $m^{-3}$ to 11.3 µg $m^{-3}$ as the distance from the roadway increased from the 100m to the 610m centroid group. There was a decrease of approximately 1 µg $m^{-3}$ between the 100m and 240m centroid groups and another decrease of 1 µg $m^{-3}$ between the 240m and 430m groups, indicating a gradual reduction in traffic-related $PM_{2.5}$ emissions as the distance from the roadway increased. The 430m and 610m downwind concentrations were 11.8 µg $m^{-3}$ and 11.3 µg $m^{-3}$, respectively, and the decrease between these two groups was only 0.5 µg $m^{-3}$. These findings suggest that the $PM_{2.5}$ emissions related to traffic slowly decrease with distance.

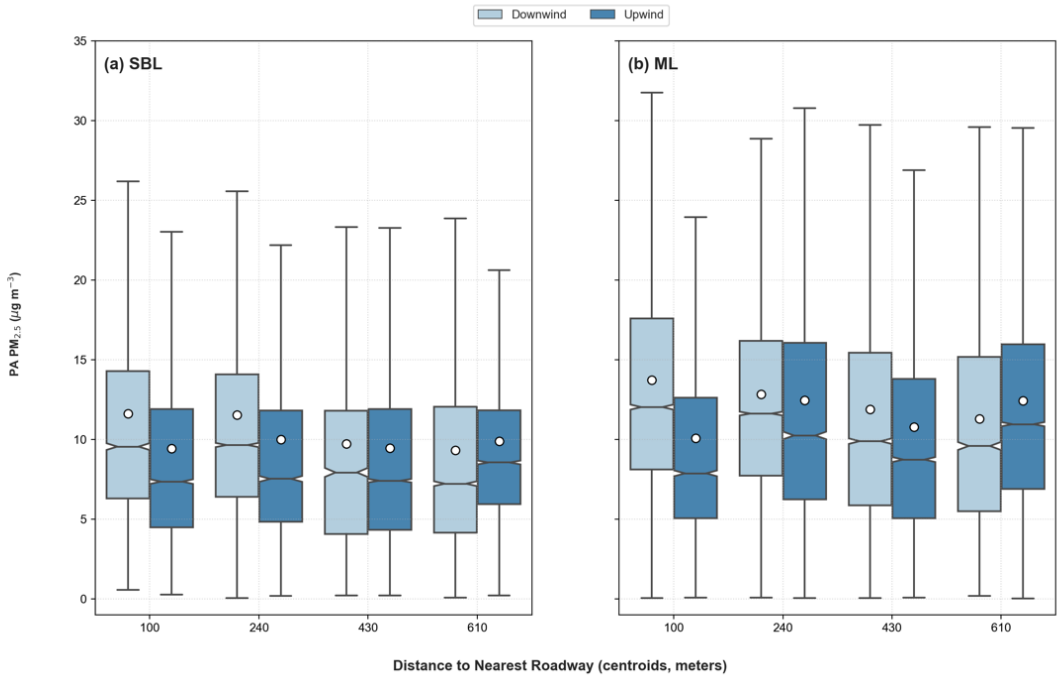


Figure 4.6: Boxplot of $PM_{2.5}$ concentrations (µg $m^{-3}$) with the distance to the nearest roadway for downwind and upwind cases for (a) stable boundary layer conditions and (b) mixed layer conditions.

# CHAPTER 5

## Conclusion

In this paper we present a preliminary investigation into the impact of roadway activities on $PM_{2.5}$ concentrations using low-cost sensor networks in Los Angeles, California. By incorporating meteorological and traffic data, we gained insights into the spatial and temporal variation of $PM_{2.5}$ with distance from the roadways. The results indicate that the $PM_{2.5}$ concentrations were elevated within 240 meters of the roadway and decayed to the background concentration by 430 meters. The concentrations were 24% and 16% higher than the mean background concentration for PA sensors in the 100m and 240m centroid groups, respectively. During SBL conditions, the concentrations of $PM_{2.5}$ near roadways led to a 20% increase in downwind concentrations compared to the SBL background, extending up to 240 meters from the roadways.

Furthermore, under periods of high atmospheric stability and low wind speeds, high traffic flow contributed to the accumulation of $PM_{2.5}$ near roadways. During ML conditions, the downwind concentrations of $PM_{2.5}$ were 18% and 10% higher than ML background for the 100m and 240m centroid groups, respectively. Despite the higher traffic flow observed during ML conditions in the 240m group, the elevation in $PM_{2.5}$ concentration was not more significant than that observed during SBL conditions. This finding suggests that high wind speeds and low atmospheric stability during ML conditions facilitate the dilution of traffic-related $PM_{2.5}$.

# References


Anderson, J. O., Thundiyil, J. G., & Stolbach, A. (2012). Clearing the Air: A Review of the Effects of Particulate Matter Air Pollution on Human Health. *Journal of Medical Toxicology*, *8*(2), 166–175. https://doi.org/10.1007/s13181-011-0203-1

AQ-SPEC. (2019). the Air Quality Sensor Performance Evaluation Center: PurpleAir PA-II evaluation summary. http://www.aqmd.gov/docs/default-source/aq-spec/summary/purpleair-pa-ii---summary-report.pdf?sfvrsn=4/

Askariyeh, M. H., Zietsman, J., & Autenrieth, R. L. (2020). Traffic contribution to PM2.5 increment in the near-road environment. *Atmospheric Environment*, *224*, 117113. https://doi.org/10.1016/j.atmosenv.2019.117113

Barkjohn, K. J., Gantt, B., & Clements, A. D. (2021). Development and application of a United States-wide correction for PM<sub>2.5</sub> data collected with the PurpleAir sensor. *Atmospheric Measurement Techniques*, *14*(6), 4617–4637. https://doi.org/10.5194/amt-14-4617-2021

Bi, J., Stowell, J. D., Seto, E., English, P., Al-Hamdan, M. Z., Kinney, P. L., Freedman, F. R., & Liu, Y. (2020b). Contribution of low-cost sensor measurements to the prediction of PM2.5 levels: A case study in Imperial County, California, USA. *Environmental Research*, *180*, 108810. https://doi.org/10.1016/j.envres.2019.108810

Brugge, D., Durant, J. L., & Rioux, C. (2007). Near-highway pollutants in motor vehicle exhaust: A review of epidemiologic evidence of cardiac and pulmonary health risks. *Environmental Health*, *6*(1). https://doi.org/10.1186/1476-069x-6-23

Bulot, F. M. J., Russell, H. S., Rezaei, M., Johnson, M. P., Johnston, S. J., Morris, A. P., Basford, P. J., Easton, N. H. C., Foster, G. L., Loxham, M., & Cox, S. R. (2020). Laboratory Comparison of Low-Cost Particulate Matter Sensors to Measure Transient Events of Pollution. *Sensors*, *20*(8), 2219. https://doi.org/10.3390/s20082219

Choi, W., He, M., Barbesant, V., Kozawa, K., Mara, S., Winer, A. M., & Paulson, S. E. (2012). Prevalence of wide area impacts downwind of freeways under pre-sunrise stable atmospheric conditions. *Atmospheric Environment*, *62*, 318–327. https://doi.org/10.1016/j.atmosenv.2012.07.084

Choi, W., Winer, A. M., & Paulson, S. E. (2014). Factors controlling pollutant plume length downwind of major roadways in nocturnal surface inversions. *Atmospheric Chemistry and Physics*, *14*(13), 6925–6940. https://doi.org/10.5194/acp-14-6925-2014

Clements, A. D., Griswold, W. G., Rs, A., Johnston, J. E., Herting, M. M., Thorson, J., Collier-Oxandale, A., & Hannigan, M. P. (2017). Low-Cost Air Quality Monitoring Tools: From

Research to Practice (A Workshop Summary). *Sensors*, *17*(11), 2478. https://doi.org/10.3390/s17112478

Feenstra, B., Papapostolou, V., Hasheminassab, S., Zhang, H., Boghossian, B. D., Cocker, D. R., & Polidori, A. (2019). Performance evaluation of twelve low-cost PM2.5 sensors at an ambient air monitoring site. *Atmospheric Environment*, *216*, 116946. https://doi.org/10.1016/j.atmosenv.2019.116946

Gupta, P. K., Doraiswamy, P. M., Levy, R., Pikelnaya, O., Maibach, J., Feenstra, B., Polidori, A., Kiros, F., & Mills, K. I. (2018). Impact of California Fires on Local and Regional Air Quality: The Role of a Low-Cost Sensor Network and Satellite Observations. *Geohealth*, *2*(6), 172–181. https://doi.org/10.1029/2018gh000136

Harrison, R. M., Jones, A. M., Gietl, J. K., Yin, J., & Green, D. (2012). Estimation of the Contributions of Brake Dust, Tire Wear, and Resuspension to Nonexhaust Traffic Particles Derived from Atmospheric Measurements. *Environmental Science & Technology*, *46*(12), 6523–6529. https://doi.org/10.1021/es300894r

HEI. (2010). Traffic-related air pollution: a critical review of the literature on emissions, exposure, and health effects. https://www.healtheffects.org/publication/traffic-related-air-pollution-critical-review-literature-emissions-exposure-and-health/

Hoek, G., Brunekreef, B., Goldbohm, S., Fischer, P., & Van Den Brandt, P. A. (2002). Association between mortality and indicators of traffic-related air pollution in the Netherlands: a cohort study. *The Lancet*, *360*(9341), 1203–1209. https://doi.org/10.1016/s0140-6736(02)11280-3

Hu, S., Fruin, S., Kozawa, K., Mara, S., Paulson, S. E., & Winer, A. M. (2009). A wide area of air pollutant impact downwind of a freeway during pre-sunrise hours. *Atmospheric Environment*, *43*(16), 2541–2549. https://doi.org/10.1016/j.atmosenv.2009.02.033

IBM. (2019). The Weather Company (IBM), 2019. The Weather Underground – Wundermap. https://www.wunderground.com/wundermap

Janssen, N. A., Brunekreef, B., Van Vliet, P., Aarts, F., Meliefste, K., Harssema, H., & Fischer, P. (2003). The relationship between air pollution from heavy traffic and allergic sensitization, bronchial hyperresponsiveness, and respiratory symptoms in Dutch schoolchildren. *Environmental Health Perspectives*, *111*(12), 1512–1518. https://doi.org/10.1289/ehp.6243

Jeong, C. H., Wang, J. M., Hilker, N., Debosz, J., Sofowote, U., Su, Y., Noble, M., Healy, R. M., Munoz, T., Dabek-Zlotorzynska, E., Celo, V., White, L., Audette, C., Herod, D., & Evans, G. J. (2019). Temporal and spatial variability of traffic-related PM2.5 sources: Comparison of exhaust and non-exhaust emissions. *Atmospheric Environment*, *198*, 55–69. https://doi.org/10.1016/j.atmosenv.2018.10.038

Karner, A., Eisinger, D. S., & Niemeier, D. A. (2010). Near-Roadway Air Quality: Synthesizing the Findings from Real-World Data. *Environmental Science & Technology*, *44*(14), 5334–5344. https://doi.org/10.1021/es100008x

Magi, B. I., Cupini, C., Francis, J., Green, M. A., & Hauser, C. D. (2020). Evaluation of PM2.5 measured in an urban setting using a low-cost optical particle counter and a Federal Equivalent Method Beta Attenuation Monitor. *Aerosol Science and Technology*, *54*(2), 147–159. https://doi.org/10.1080/02786826.2019.1619915

McCarthy, M., Eisinger, D. S., Hafner, H. R., Chinkin, L. R., Roberts, P. H., Black, K. J., Clark, N. N., McMurry, P. H., & Winer, A. M. (2006). Particulate Matter: A Strategic Vision for Transportation-Related Research. *Environmental Science & Technology*, *40*(18), 5593–5599. https://doi.org/10.1021/es062767i

Oroumiyeh, F., Jerrett, M., Del Rosario, I., Lipsitt, J., Liu, J. T. C., Paulson, S. E., Ritz, B., Schauer, J. J., Shafer, M. M., Shen, J., Weichenthal, S., Banerjee, S., & Zhu, Y. (2022). Elemental composition of fine and coarse particles across the greater Los Angeles area: Spatial variation and contributing sources. *Environmental Pollution*, *292*, 118356. https://doi.org/10.1016/j.envpol.2021.118356

Pearson, R. R., Wachtel, H., & Ebi, K. L. (2000). Distance-Weighted Traffic Density in Proximity to a Home Is a Risk Factor for Leukemia and Other Childhood Cancers. *Journal of the Air & Waste Management Association*, *50*(2), 175–180. https://doi.org/10.1080/10473289.2000.10463998

Pope, C., & Dockery, D. W. (2006). Health Effects of Fine Particulate Air Pollution: Lines that Connect. *Journal of the Air & Waste Management Association*, *56*(6), 709–742. https://doi.org/10.1080/10473289.2006.10464485

Puett, R. C., Hart, J. E., Schwartz, J., Hu, F. B., Liese, A. D., & Laden, F. (2010). Are Particulate Matter Exposures Associated with Risk of Type 2 Diabetes? *Environmental Health Perspectives*, *119*(3), 384–389. https://doi.org/10.1289/ehp.1002344

PurpleAir. (2022). Real-Time Air Quality Map | PurpleAir. Real-Time Air Quality Map | PurpleAir. https://map.purpleair.com/

Ranasinghe, D., Lee, E. S., Zhu, Y., Frausto-Vicencio, I., Choi, W., Sun, W., Mara, S., Seibt, U., & Paulson, S. E. (2019). Effectiveness of vegetation and sound wall-vegetation combination barriers on pollution dispersion from freeways under early morning conditions. *Science of the Total Environment*, *658*, 1549–1558. https://doi.org/10.1016/j.scitotenv.2018.12.159

Rowangould, G. (2013). A census of the US near-roadway population: Public health and environmental justice considerations. *Transportation Research Part D-Transport and Environment*, *25*, 59–67. https://doi.org/10.1016/j.trd.2013.08.003

Rutter, A. P., Snyder, D. S., Schauer, J. J., Sheesley, R. J., Olson, M. F., & DeMinter, J. (2011). Contributions of resuspended soil and road dust to organic carbon in fine particulate matter in the Midwestern US. *Atmospheric Environment*. https://doi.org/10.1016/j.atmosenv.2010.10.014

Sayahi, T., Butterfield, A., & Kelly, K. (2019). Long-term field evaluation of the Plantower PMS low-cost particulate matter sensors. *Environmental Pollution*, *245*, 932–940. https://doi.org/10.1016/j.envpol.2018.11.065

South Coast Air Quality Management District. (2022). South coast AQMD air quality sensor performance evaluation center: Summary tables and reports. Retrieved August 12, 2022, from http://www.aqmd.gov/aq-spec/evaluations/summary-pm

Tryner, J., Mehaffy, J., Miller-Lionberg, D., & Volckens, J. (2020). Effects of aerosol type and simulated aging on performance of low-cost PM sensors. *Journal of Aerosol Science*, *150*, 105654. https://doi.org/10.1016/j.jaerosci.2020.105654

US Census Bureau. (2020). U.S. Census Bureau QuickFacts: Los Angeles County, California. Census Bureau QuickFacts. https://www.census.gov/quickfacts/losangelescountycalifornia

Van Der Vliet, P. C., Knape, M., De Hartog, J. J., Janssen, N., Harssema, H., & Brunekreef, B. (1997). Motor Vehicle Exhaust and Chronic Respiratory Symptoms in Children Living near Freeways. *Environmental Research*, *74*(2), 122–132. https://doi.org/10.1006/enrs.1997.3757

Wallace, L., Bi, J., Ott, W. R., Sarnat, J. A., & Liu, Y. (2021). Calibration of low-cost PurpleAir outdoor monitors using an improved method of calculating PM. *Atmospheric Environment*, *256*, 118432. https://doi.org/10.1016/j.atmosenv.2021.118432

Williams, L. A., Ulrich, C. M., Larson, T. V., Wener, M. H., Wood, B. L., Campbell, P. J., Potter, J. D., McTiernan, A., & De Roos, A. J. (2009). Proximity to Traffic, Inflammation, and Immune Function among Women in the Seattle, Washington, Area. *Environmental Health Perspectives*, *117*(3), 373–378. https://doi.org/10.1289/ehp.11580

Yong, Z., & Haoxin, Z. (2016). Digital universal particle concentration sensor: PMS5003 series data manual (2016 product data manual of PLANTOWER). (2016). https://www.aqmd.gov/docs/default-source/aq-spec/resources-page/plantower-pms5003-manual_v2-3.pdf/